

# Assessment of the Quirónsalud Proton Therapy Centre Accelerator for Single Event Effects Testing

Andrea Coronetti, *Associate Member, IEEE*, Natalia Emriskova, Rubén García Alía, *Member, IEEE*, Juan Antonio Vera Sanchez, Alejandro Mazal

**Abstract**—High-energy proton testing is used for single-event effect (SEE) qualification of electronics to be used in several radiation harsh environments. Given the increasing demand, exploiting the capabilities of proton therapy centres for electronics testing may become desirable. In this paper the focus is on the Quirónsalud proton therapy centre, which makes use of a synchrocyclotron to accelerate protons within an energy range of 70-226 MeV. Lower energies can be obtained with degradation. The use of a synchrocyclotron may pose unique challenges for SEE testing, as opposed to the use of a cyclotron, because the time structure of the beam is very complex and very intense instantaneous fluxes are delivered in highly localized areas of the device under test. Independent characterization measurements of the beam time structure and the beam uniformity were performed. SEE testing on some golden chips previously characterized in cyclotron facilities were also accomplished. These showed that the single-event upset (SEU) cross sections measured with this beam are in good agreement with those measured at cyclotrons in the 20-226 MeV proton energy range. As demonstrated by the SEU cross-sections and by the analysis of multiple-cell upsets (MCU), no beam pulse effects are observed that can alter the data collection on the chips despite the very intense instantaneous fluxes. A few limitations were also evidenced when testing with energies below 20 MeV and due to the fixed flux for testing.

**Index Terms**—Single-event effects, high-energy protons, accelerator, pulsed beam effects, silicon diode dosimetry.

## I. INTRODUCTION

HIGH-energy proton single-event effect (SEE) testing and qualification are employed in many application fields, ranging from space [1], accelerator [2] and even for high-reliability ground-level applications (e.g., automotive) [3], as a proxy to neutron irradiation. For all these cases, SEE testing must be conducted with accelerators capable of delivering to the device under test (DUT) protons with energies in the 20-200 MeV range.

In Europe, two reference facilities for these irradiation conditions are the Paul Scherrer Institute (PSI) [4], in Switzerland, and the University Medical Center of Groningen (UMCG) [5], in the Netherlands. Similar infrastructures exist outside

This study has received funding from the European Union's Horizon 2020 research and innovation programme under grant agreement no. 101008126.

Andrea Coronetti (andrea.coronetti@cern.ch) is with CERN, CH-1211 Geneva, Switzerland and with Institute d'Électronique et des Systèmes, Université de Montpellier, 34090 Montpellier, France.

Natalia Emriskova and Rubén García Alía are with CERN, CH-1211 Geneva 23, Switzerland.

Juan Antonio Vera Sanchez and Alejandro Mazal are with Quirónsalud Proton Therapy Centre, 28223 Pozuelo de Alarcón, Spain.

of Europe and given the high demand, in the United States the possibility to exploit proton therapy centres for electronics testing has been deeply explored in the last decade. Considerations on demand and fragility of the established facility network have brought also the European Space Agency (ESA) to consider the exploitation of proton therapy centres, such as the one in Delft, in the Netherlands [6].

Given the harsh qualification requirements for the high-luminosity large hadron collider upgrade, CERN is also facing an increasing internal demand for SEE qualification and lot acceptance tests in the coming years. Therefore, after screening through the proton therapy centres available in Europe, that managed by Quirónsalud near Madrid, Spain, has been selected to perform an assessment of its suitability for radiation effects testing of electronics. This assessment includes an evaluation of the beam parameters and of the test instrumentation available at the facility, an independent beam characterization, as well as actual SEE tests on memory devices. One crucial point is to assess whether the pulsed time structure and beam scanning have an impact on the SEE measurements when compared to cyclotron-based facilities, where the beam is often continuous and delivered uniformly over a wide surface.

This paper provides a description of the facility for future reference as well as of the beam characteristics. It then reports the details of the beam characterization and SEE measurements performed by CERN and their comparison with the data collected at other European proton facilities.

## II. FACILITY DESCRIPTION

The Quirónsalud proton therapy centre is located in Pozuelo de Alarcón, Madrid, Spain. Protons are accelerated by means of a S2C2 synchrocyclotron mounted in a Proteus One machine provided by IBA (Louvain-la-neuve, Belgium). The achievable energy range from machine tuning and degradation is 2.5-226 MeV, making it suitable not only for standard proton testing, but also for direct proton ionization studies [7–13].

The synchrocyclotron gantry is mounted on the top of the irradiation room above the ceiling. The gantry can be rotated over an angle of 220° allowing the best suited geometry configuration for various types of tests. In this experiment, the beam is delivered from top to bottom, as indicated in Fig. 1, at normal incidence on the devices. The beam crosses a system composed of two consecutive ionization chambers, out of which only the external one is visible in Fig. 1. These

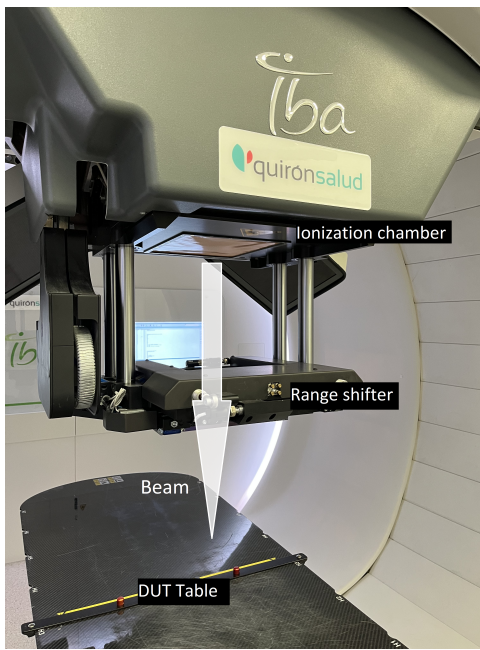


Fig. 1. Irradiation area at the Quirónsalud proton therapy centre. The synchrocyclotron is positioned at the top of the room and the beam is directed from top to bottom.

are used to measure the spot dose and position of the beam and, therefore, the proton fluence.

The primary energy of the beam is tunable in the 70-226 MeV energy range. All energies in this range can be achieved without the need for a downstream degrader. A range shifter, or beam energy degrader, can also be inserted to change the energy at the DUT position and obtain energies lower than 70 MeV. During these experiments, the energy was reduced down to 2.5 MeV, degraded from a primary energy of 70 MeV. Note that the beam is no longer mono-energetic, so this value must be considered as the average energy of a wider distribution. The beam energy degrader is a 35 mm thick polycarbonate plate with a density of 1.2 g/cm<sup>3</sup>. This is the only degrader currently employed, therefore, energy reduction is obtained with a combined primary energy tuning. The air distance between the exit of the nozzle and the DUT measured to be 110 cm. Irradiation was performed in air and the energies reported hereafter are those at the DUT position. Therefore, they are measured after the further energy degradation in the air for the lowest energies.

The machine is tuned for patient treatment, so it is set to deliver the dose over millimetric spots. However, the beam can be scanned over a rather large area while preserving its spatial uniformity, ensuring a < 1% uncertainty on the delivered dose, which is better than what is required by standards for electronics testing (< 10%).

The proton flux, the beam spot size and the low-frequency time structure of the beam all change with the primary beam energy. Typically, when lower energies are set, the proton flux reduces, the beam spot size enlarges and, consequently, the dose rate decreases and longer irradiation times are needed to achieve the same fluence. The beam spot has a Gaussian shape,

TABLE I  
INSTANTANEOUS AND AVERAGE PROTON FLUXES AS A FUNCTION OF THE ENERGY OF THE BEAM.

Energy [MeV]	Max. Inst. Flux in a spot [p/cm <sup>2</sup> /s]	Avg. Flux in a spot [p/cm <sup>2</sup> /s]
226	$3.63 \times 10^{11}$	$2.93 \times 10^9$
150	$1.52 \times 10^{11}$	$1.54 \times 10^9$
100	$4.55 \times 10^{10}$	$6.17 \times 10^8$
50	$1.45 \times 10^{10}$	$3.53 \times 10^8$
20	$4.09 \times 10^9$	$2.20 \times 10^8$
9	$3.79 \times 10^9$	$2.05 \times 10^8$
6	$3.65 \times 10^9$	$1.95 \times 10^8$
2.5	$3.54 \times 10^9$	$1.77 \times 10^8$

with a sigma of 3 mm in both directions, when the energy is tuned to 226 MeV in air. At the primary energy of 70 MeV the beam spot sigma becomes 7 mm wide. The largest beam size that can be attained is 20×24 cm<sup>2</sup>. Therefore, the facility can be used for component-level characterization as well as to irradiate full boards or systems.

The proton beam is delivered in each spot in  $\sim 7 \mu\text{s}$ . Therefore, the instantaneous proton flux is a few orders of magnitude higher than the average proton flux. Beam scanning allowed covering a surface of 3×3 cm<sup>2</sup> in a uniform manner. The scanning surface size is independent of the beam energy. The scanning is achieved by depositing the beam over 169 spots (arranged in 13 rows and 13 columns) that are spaced 2.3 mm apart.

Depending on the demanded fluence, it may be necessary to deliver beam to each spot multiple times. If needed, each spot is therefore re-irradiated at intervals of 1 ms. Once the fluence on a certain spot is reached, the next adjacent spot is targeted and irradiated. The time to move to the next spot is again 1 ms. The scanning over the whole grid depends on the fluence that is targeted. If, for instance, the fluence can be reached in a single irradiation, then the 169 spot grid is covered in 169 ms. However, it is more likely that the total fluence in a spot cannot be achieved by a single spot irradiation, therefore, the irradiation on a single spot may be repeated multiple times. When degraders are employed, there is a loss of beam particles that must be compensated for by multiple irradiations over the same spot. Therefore, the time to cover the full grid can reach tens of seconds. Note that the  $\sim 7 \mu\text{s}$  pulse duration and the 1 ms dead time between two irradiation, whether in the same or the next spot, do not vary with the primary beam energy.

Tuning of the flux is currently not available, so all tests must be carried out at certain fixed fluxes that varies with the energy of the beam. In the following, the instantaneous flux is taken as that delivered in each spot during the 7  $\mu\text{s}$  and measured by the facility ionization chamber. The facility provides a measurement of the dose in monitor units, which can be first converted in a dose in water and then into a proton fluence by considering the size of the beam and the stopping power of the protons. Then, the instantaneous flux in a spot is calculated by dividing by the 7  $\mu\text{s}$  spill duration. The average flux in a spot reported hereafter is based on the total fluence delivered in a spot over the full irradiation (measured by the ionization chamber) divided by the total time of irradiation.

As shown in Table I, the maximum instantaneous flux in

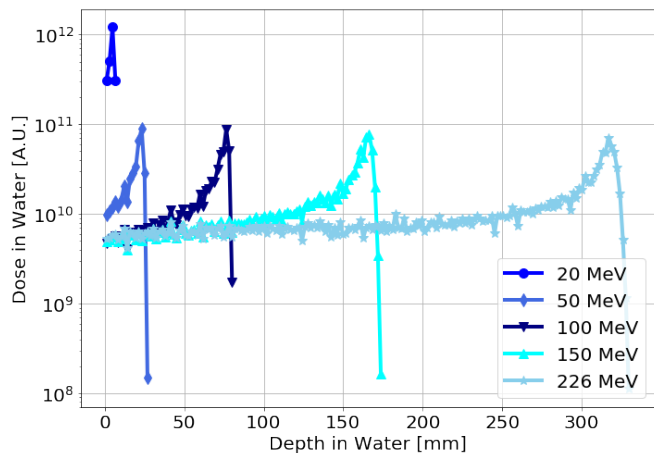


Fig. 2. Dose-depth curves in water for various proton energies measured with the MLIC.

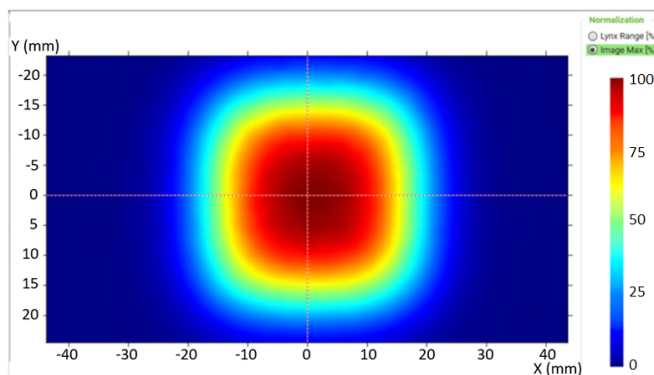


Fig. 3. Measurement of beam uniformity over the whole beam size obtained with a scintillator at a primary beam energy of 100 MeV. The colorscale provides a normalization of the beam intensity at the various points based on the maximum value. The map shows that a uniformity within  $\pm 10\%$  can be achieved over an area of  $\sim 2 \times 2 \text{ cm}^2$ .

a spot is very high due to the very short spill duration and, to a lesser extent, due to the small beam spot size. For the same reason, the actual number of protons deposited in a spot within a spill is  $< 10^6$ . The average flux in a spot is in the order of  $10^8$ - $10^9 \text{ p/cm}^2/\text{s}$ , which is typically the maximum flux that one would like to have in a high-energy proton test and it is also the maximum flux achievable at PSI and UMG for beam sizes of the order of  $2 \times 2 \text{ cm}^2$ .

The energy of the proton beam was calibrated through dose-depth curves measured at the DUT position. These are obtained by means of a multi-layer ionization chamber (MLIC) that is positioned at the beam exit window and allow measuring the Bragg peak in water of the proton beam. Fig. 2 shows the dose-depth curves in water measured for some of the energies used during the tests here reported.

The beam uniformity over the whole beam size, and obtained through beam scanning, was assessed by means of a scintillator screen and it is reported in Fig. 3 for the 100 MeV case. The colorscale reports the normalized intensity of the beam with respect to the maximum. The measurement shows that a uniformity within  $\pm 10\%$  was achieved for an area of  $\sim 2 \times 2 \text{ cm}^2$ .

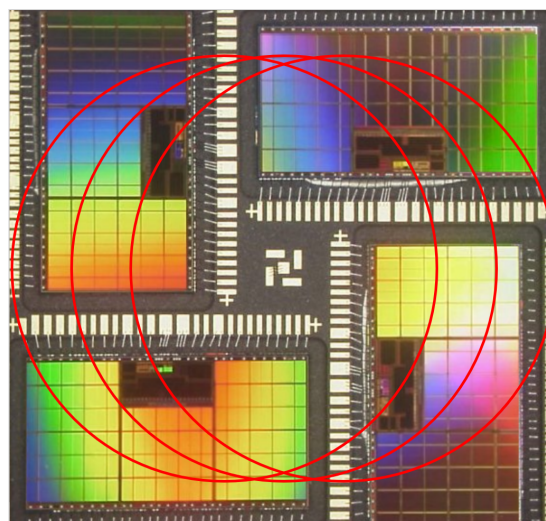


Fig. 4. Projections of beam spot sizes on top of the ESA Monitor for three adjacent beam spots. The FWHM of each spot is shown with red circles and it is based on the 7 mm sigma for the 2.5-70 MeV energy range.

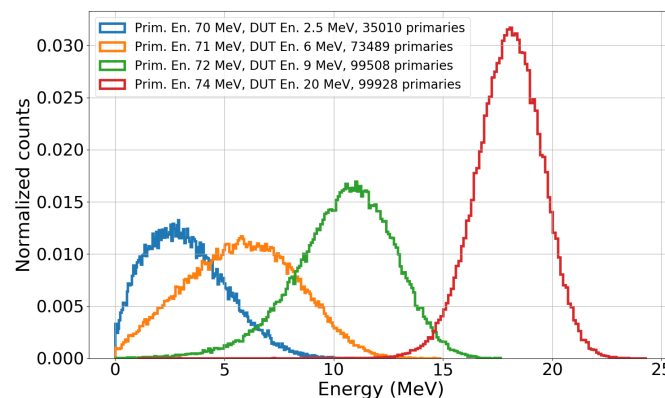


Fig. 5. TRIM simulations of the proton spectra received at the DUT when degrading the proton beam with the range shifter. The legend shows the primary proton energy, the energy at the DUT and the number of primaries that made it to the DUT. Number of primaries for all simulations was set to  $10^5$ , except for the 2.5 MeV for which  $5 \times 10^5$  primaries were simulated.

Fig. 4 shows the projections of single beam spot sizes over the areas of an ESA Monitor, which is  $2 \times 2 \text{ cm}^2$  wide. The red circles have a diameter corresponding to the full width at half maximum (FWHM) of the spot and the depicted case was that with the largest beam spot sizes, i.e., for all energies below 20 MeV. Three adjacent spots are depicted, showing that a single spot already provides a very wide coverage of the surface of a very large die. Therefore, in the case of millimetric size dies, scanning of the beam spot may not even be needed to achieve the required uniformity.

The TRIM tool of the SRIM package [14] was used to simulate the transport of the protons through the range shifter (degrader) and the layers of air that stood between the primary beam exiting the nozzle of the accelerator and the DUT. As said, the range shifter is 35 mm thick and has a density of  $1.2 \text{ g/cm}^3$ . The two layers of air before and after the range shifter have a total thickness of 110 cm. The degraded energies of 2.5, 6, 9 and 20 MeV were obtained with the same range

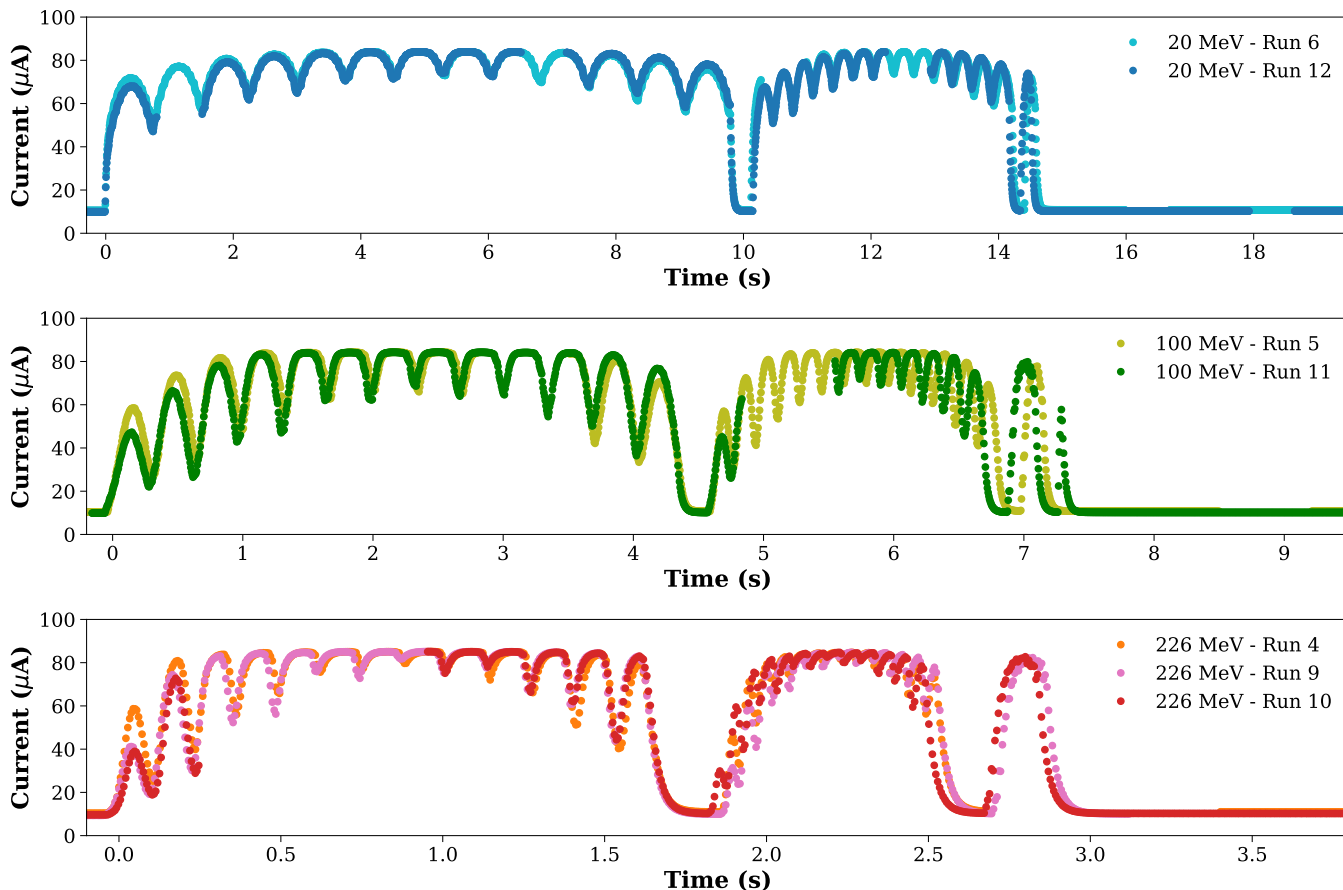


Fig. 6. Proton beam time profiles as measured by the silicon diode and the SMU, for various runs with beam energies of 20 MeV (top), 100 MeV (middle) and 226 MeV (bottom), for the same proton fluence. Some data-points are missing due to the logging dead time of the SMU with little loss of information.

shifter starting from primary proton beam energies at the beam exit window of 70, 71, 72 and 74 MeV.

The TRIM simulations employed  $10^5$  primaries ( $5 \times 10^5$  for the lowest energy case). The results of these simulations in terms of degraded proton spectra are depicted in Fig. 5. As shown in the legend of the figure, some loss of beam particles occur when trying to achieve the lowest energies. In all other cases, the beam fluence is preserved with very minimal uncertainty. Concerning the spectra, as expected, they become wider when the primary energy of the beam is reduced due to the higher effectiveness of the degrading material. The spectra have an increasingly large FWHM when the energy is reduced. The simulations provide central values for these spectra that can be slightly different from those measured with the MLIC. For the expected 20 MeV the simulated energy was 18.5 MeV, for the expected 9 MeV it was 11 MeV, for the expected 6 MeV it was 7 MeV and for the expected 2.5 MeV it was 3 MeV. However, simulations may be affected by uncertainties when the particles are close to their end of range. The same can happen to the experimental instrumentation used to measure the energy.

### III. BEAM CHARACTERIZATION MEASUREMENTS

A silicon diode from Canberra, model PD 300-16-1000 AM, was used to perform measurements

of the beam time profile as it would be seen by an actual electronic device. The active volume of this diode is cylindrical with a surface of  $300 \text{ mm}^2$  and thickness of 1 mm. The diode was biased at 200 V by a Source Measurement Unit (SMU) Keithley 2410. The use of this type of diode for beam characterization has been presented before [15–18]. The signal generated in the diode is amplified using a CIVIDEC model C1HV0091 with 21.9 dB gain and then digitized using a CAEN DT5751.

The logging of the SMU current allows capturing the long time structures of the beam. This current is a function of the photocurrent induced by the protons interacting with the silicon diode. The sampling frequency of the SMU was 180 Hz and the current compliance of the SMU was set to  $100 \mu\text{A}$  and therefore not reached during the measurements. The saturation visible in Fig. 6 at  $\sim 80 \mu\text{A}$  is caused by the protection resistance of the pre-amplifier which limits the current. Bias voltage on the diode is not affected because the SMU is not saturating and is set to provide the correct bias.

The SMU logging could capture the time structure related to a complete irradiation. These long time structures are depicted in Fig. 6 for three different energies ranging from 20 to 226 MeV. This shows that, overall, the beam is delivered in at least three passages that are separated by a few hundreds ms break. These three longest structures have increasingly

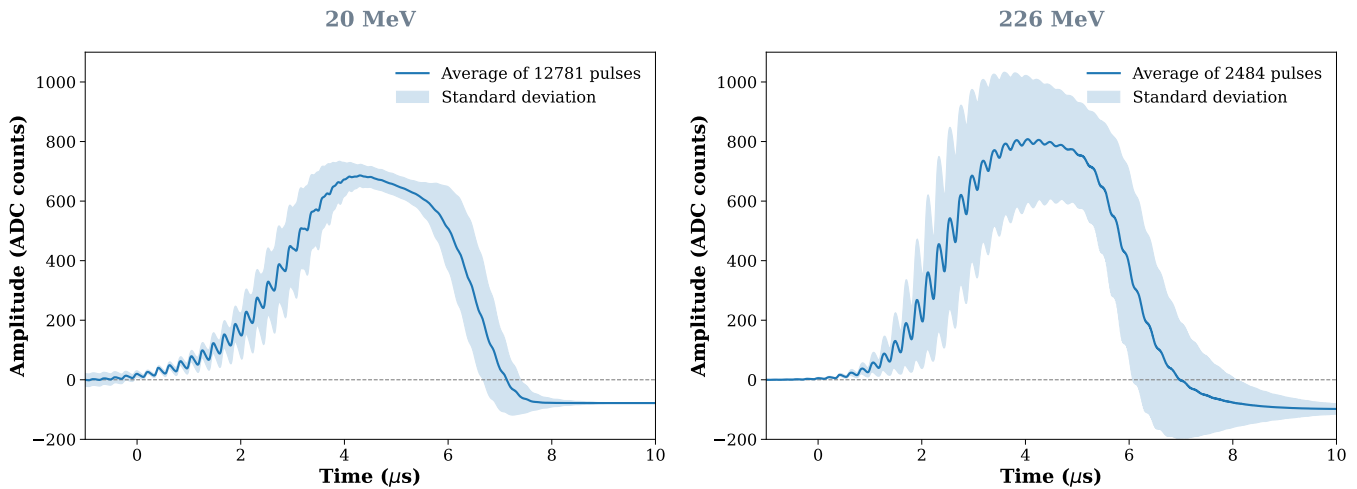


Fig. 7. Average spot pulse time structure as measured by the silicon diode, for a proton energy of 20 MeV (left) and 226 MeV (right).

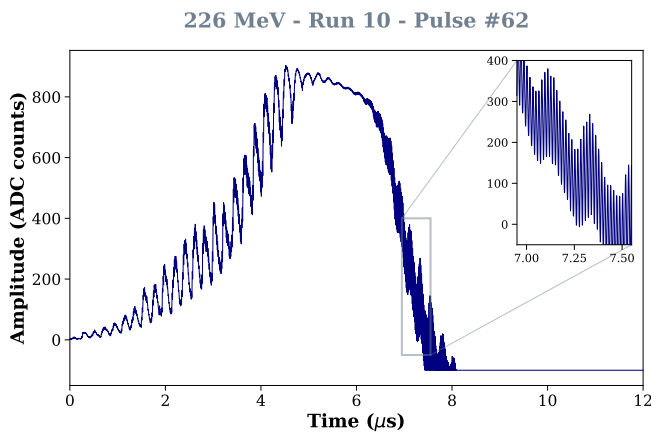


Fig. 8. Example of a single spot pulse for the 226 MeV proton beam.

lower duration. They are a consequence of the "blind golfer" algorithm. This algorithm is used in proton therapy to ensure the best possible uniformity in terms of dose delivered to each spot. All 169 beam spots are irradiated at least once within each of these three time structures. To better explain how this works, the 226 MeV case is explained in deeper detail. For this case, each spot is irradiated 10 times during the first longest time structure, 4 times during the second longest time structure and a single time during the shortest time structure. For this reason, the first time structure is completed in 1.69 s, i.e., 169 spots irradiated 10 times at a frequency of 1 ms. For lower energies, the blind golfer algorithm principle is the same, but the 169 spots need to be irradiated even 30 or 60 times within the first longest time structure to achieve the same fluence as in the 226 MeV case. Therefore, the time to complete the irradiation may increase by up to 6 times.

A second, faster, time structure that can be observed from this same figure is related to the beam scanning and would not be visible if scanning was not employed. In both the first and second longest time structures 13 shorter structures are visible that are related to the scanning of the 13 rows. On the other

hand, the column scanning is not resolved in this measurement. For the shortest time structure of the blind golfer algorithm, row scanning is also not resolved due to the fact that each spot is irradiated just once and then the beam keeps moving over the spot grid within just a few hundreds ms. Since the scanning is performed over a wider surface than the diode surface, only a fraction of the beam actually reach the sensitive area of the diode at the edges of the row scanning, that is the reason why there are some dips that highlight the presence of these 13 structures. This also explains why the saturation is reached only when scanning around the center of the diode, but not at its periphery, i.e., at the rising and falling edges of the longest time structures.

The digitization process enforced on the diode signal has a resolution as low as 1 ns. However, under the experimental conditions used in this work, the single proton pulses could not be resolved and therefore it is not possible to use single pulse energy deposition to determine the energy of the particles in the beam. This fast acquisition can nevertheless be used to capture and acquire more information on the single beam spot pulses, those lasting  $\sim 7 \mu\text{s}$ .

Fig. 7 depicts a couple of examples of average spot pulses that were measured during a 20 MeV and a 226 MeV proton energy run. There are several noteworthy aspects. The pulse duration, defined as starting 10% of maximum signal at rising edge to 10% of maximum signal at falling edge is close to  $7 \mu\text{s}$ . However, the maximum spill intensity is reached only for 1-2  $\mu\text{s}$  with very long rising and falling edges. As the two plots show, no specific energy dependency was found for the shape of the spill. Nevertheless, the spills at high energy had a lower degree of repeatability, as indicated by the larger standard deviation.

The pulse shape analysis can shed further light on even faster time structures present in the proton beam. Fig. 8 shows the time structure of a single beam spot pulse exploiting the maximum resolution of the diode. Two additional high frequency modes were captured. One of them, that has a frequency of  $\sim 250$  ns, is particularly visible on the rising edge of the pulse, but it is also present at the top and in

TABLE II  
SUMMARY OF TIME STRUCTURES PRESENT IN THE BEAM AND WHETHER THEY DEPEND ON THE PRIMARY ENERGY OF THE BEAM.

Time order of magnitude	Type of time structure	Energy dependent?
O(1)-O(10) s	Blind Golfer Algorithm	Yes
O(0.1)-O(1) s	Row scanning	Yes
O(0.01)-O(0.1) s	Column scanning	Yes
1 ms	Time between two pulses	No
$\sim 7 \mu\text{s}$	Pulse duration	No
O(10)-O(100) ns	RF bunching	No

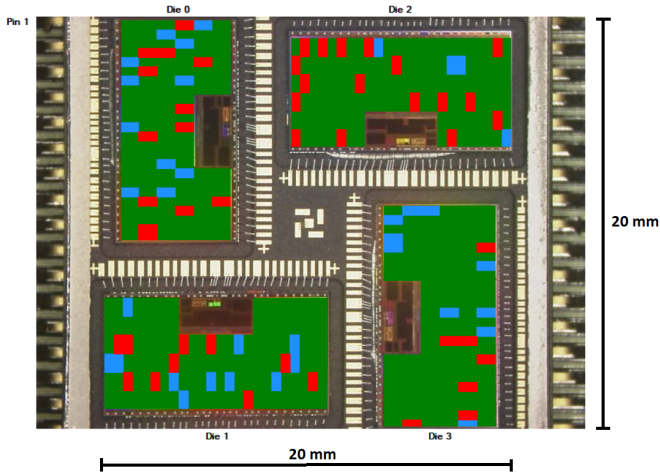


Fig. 9. Readout of the ESA monitor showing the location of the SEUs in the four memory array. Green indicates around average amount of SEUs, while red and blue an excess or a defect beyond 20%, respectively. The data ( $\sim 27000$  SEUs) were acquired during a 226 MeV run.

the falling edge. And even one faster mode is captured when zooming in on the falling edge. This faster mode seems to repeat with a frequency of  $\sim 16$  ns and is coherent with the bunching structure provided by the synchrocyclotron radio-frequency (RF) of the single shot pulse that was measured in a previous study and corresponds to 64 MHz [19]. Table II summarizes the beam time structure composition of this beam.

Other than the diode measurements of the time profile, the uniformity of the beam was assessed by means of an ESA Monitor, which is composed of four 4-Mbit static random access memories (SRAMs) from Atmel (Reference in Table III) that are arranged to cover a  $2 \times 2$  cm<sup>2</sup> surface. The ESA Monitor software can provide the physical mapping of the single-event upsets (SEUs) in the memory grid and provide information about the beam uniformity.

The data acquired during a 226 MeV proton run are reported in Fig. 9. The picture shows a typical beam distribution for a uniform beam with a majority of in-average data-points (green) and a few outliers in defect (blue) or excess (red). Given that the beam was larger than the surface of the ESA monitor, edge effects were not expected in this case. Very similar results were obtained also for the 20 MeV proton beam, as shown in Fig. 10. This is also noteworthy considering that the beam is degraded from 74 MeV, but the uniformity is mostly unaffected. These results confirm that despite the pulsed nature of the beam and the scanning of the small spot size, all areas of the chip can be reached with a sufficient uniformity to enable

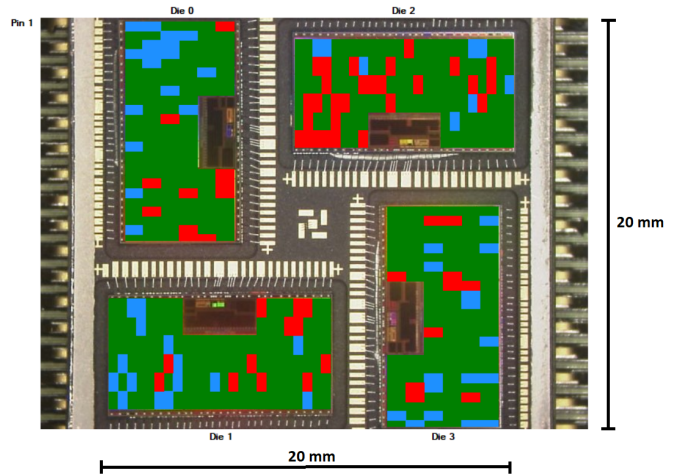


Fig. 10. Readout of the ESA monitor showing the location of the SEUs in the four memory array. Green indicates around average amount of SEUs, while red and blue an excess or a defect beyond 20%, respectively. The data ( $\sim 20000$  SEUs) were acquired during a 20 MeV run.

TABLE III  
LIST OF TESTED DEVICES AND THEIR FEATURES.

Manufacturer	Reference	Array size, Mbits	Technology, nm
Atmel	AT86166H-YM20-E	16	250
ISSI	IS61WV204816BLL	32	40
Cypress	CY62167GE30-45ZXI	16	65

SEE testing.

#### IV. SEE MEASUREMENTS AND COMPARISON WITH OTHER PROTON FACILITIES

SEU characterization on the ESA monitor and two commercial SRAMs has been performed for the purpose of verifying the correctness of the SEU cross-section measurements under this type of pulsed proton beam. A summary of the main characteristics of the three SRAMs under consideration is reported in Table III.

These SRAMs have been widely characterized in several types of beams before [13, 20, 21] and have become golden references to characterize less standard beams. The test configuration was similar to those employed elsewhere. To enable direct proton ionization testing, the SRAMs were irradiated at all energies without the package. Although, it must be remembered that the irradiation occurs with a degraded beam and in air, which may affect the resulting beam received by the devices. In addition, the Atmel SRAM (ESA Monitor) is not expected to have a direct proton ionization sensitivity, so measurements below 20 MeV had not been performed before in cyclotron facilities.

All SRAMs were biased at 3.3 V I/O and written with a checkerboard pattern. To be noted that this is a physical checkerboard only for the Atmel SRAM, whereas it is a logical checkerboard for the ISSI and Cypress SRAMs. The memories were written before beam on and then read almost continuously under beam exposure, when this was long enough. Whenever exposure lasted for less than 10 seconds,

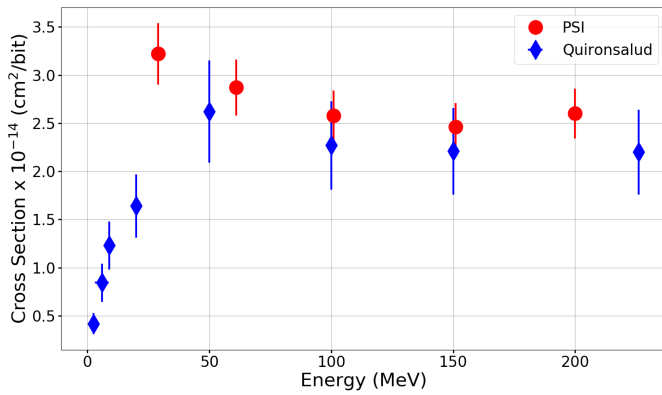


Fig. 11. Proton SEU cross sections of the ESA Monitor measured at PSI and Quirónsalud for various beam energies.

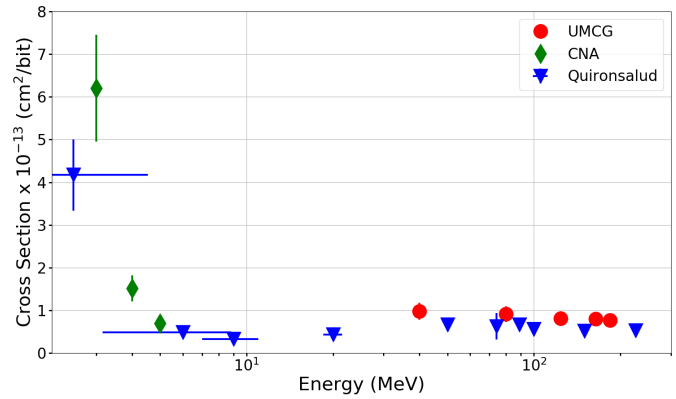


Fig. 13. Proton SEU cross sections of the Cypress measured at UMCG, CNA and Quirónsalud for various beam energies.

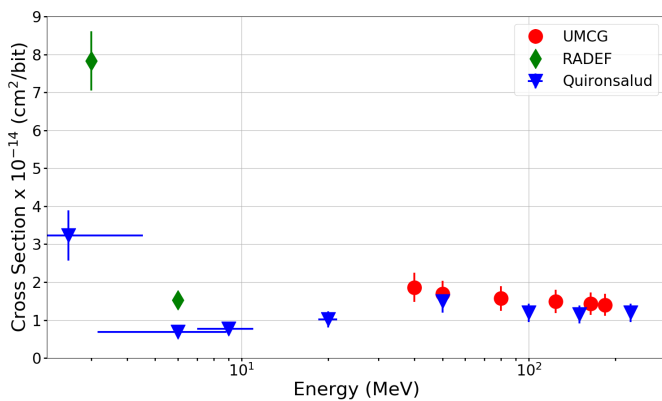


Fig. 12. Proton SEU cross sections of the ISSI measured at UMCG, RADEF and Quirónsalud for various beam energies.

the SRAMs were just read after exposure was completed. For the Atmel SRAM bits in error are not rewritten to the correct pattern, but kept in error so that the beam profile measurement function can be used. The readout was also performed at not very precise intervals and it takes about 20 seconds to complete. For the ISSI and Cypress SRAM the readout occurs at a regular frequency, each 1.5 seconds. The Cypress SRAM also has an embedded error correction code (ECC) that was disabled for the purpose of the tests.

When using a pulsed and highly concentrated beam, what one may expect is to see potential concentration of errors that may arise as a result of localized row, column or block SEFIs or micro-latchup. These may occur, in particular, when the SRAM is read during exposure, but it may occur also even for after exposure readouts for extremely pulsed beams, e.g., < ns pulse duration. As a result of these non-linear flash effects [22], the SEU cross section may erroneously be overestimated.

The SEU cross section collected for these SRAMs at Quirónsalud can be compared with those recovered elsewhere [13, 20, 21] for proton energies between 2.5 and 230 MeV. These data were collected at either PSI, UMCG, the University of Jyväskylä (RADEF) [23], in Finland, or the Centro Nacional de Aceleradores (CNA) [24], in Spain. Figs. 11-13 provide the direct SEU cross section comparison as a function of proton

energy for the three SRAMs. Error bars on cross sections are calculated with 95% confidence level and assuming a 10% uncertainty on the fluence. The latter applies to both the data collected at Quirónsalud as well as those collected at cyclotrons. Error bars for the energy of the proton beams were also added for the degraded runs from 2.5 to 20 MeV. This error bars were based on the 1-sigma of the quasi-Gaussian distributions simulated in Fig. 5.

Fig. 11 reports the SEU cross section of the ESA monitor measured as a function of the proton energy at Quirónsalud (2.5, 6, 9, 20, 50, 100, 150, 226 MeV) in comparison with the measurements performed at PSI. The data collected in both facilities fall on the same trend line. Fig. 12 reports the SEU cross section at the same energies for the commercial ISSI SRAM. In this case, the cross sections are compared with high-energy proton data collected at UMCG and with low-energy proton data collected at RADEF. At high proton energies, the Quirónsalud measurements match very well with the measurements done at UMCG, while at lower proton energies, discrepancies are observed with respect to the measurements performed at RADEF. These differences are of less than a factor of 2.5 and are likely due to the energy degradation that produces a high-energy tail in the beam at Quirónsalud, whereas for the RADEF proton beam those were mono-energetic beams (< 25 keV spread). Concerning the commercial Cypress SRAM, whose cross section is depicted in Fig. 13, the agreement is also satisfactory at both high and low energy, with the exception of an outlier. Note that the Quirónsalud SEU cross sections are on average 33% lower than those measured elsewhere for the high energies, which indicates that pulsed beam effects, such as burst of bit flips in error, were not observed.

The SEU cross sections measured for the ISSI and Cypress SRAMs at energies below 20 MeV can be compared only against a very few data points measured elsewhere. Measurements done at 2.5 MeV at Quirónsalud are typically smaller by a factor of 2-2.5 with respect to what was measured elsewhere. These same cross sections seem higher than those measured at around 5-6 MeV elsewhere. This seems to underline that there may be an effect on the measured cross section caused by the wide spectral distribution of the degraded beams. It

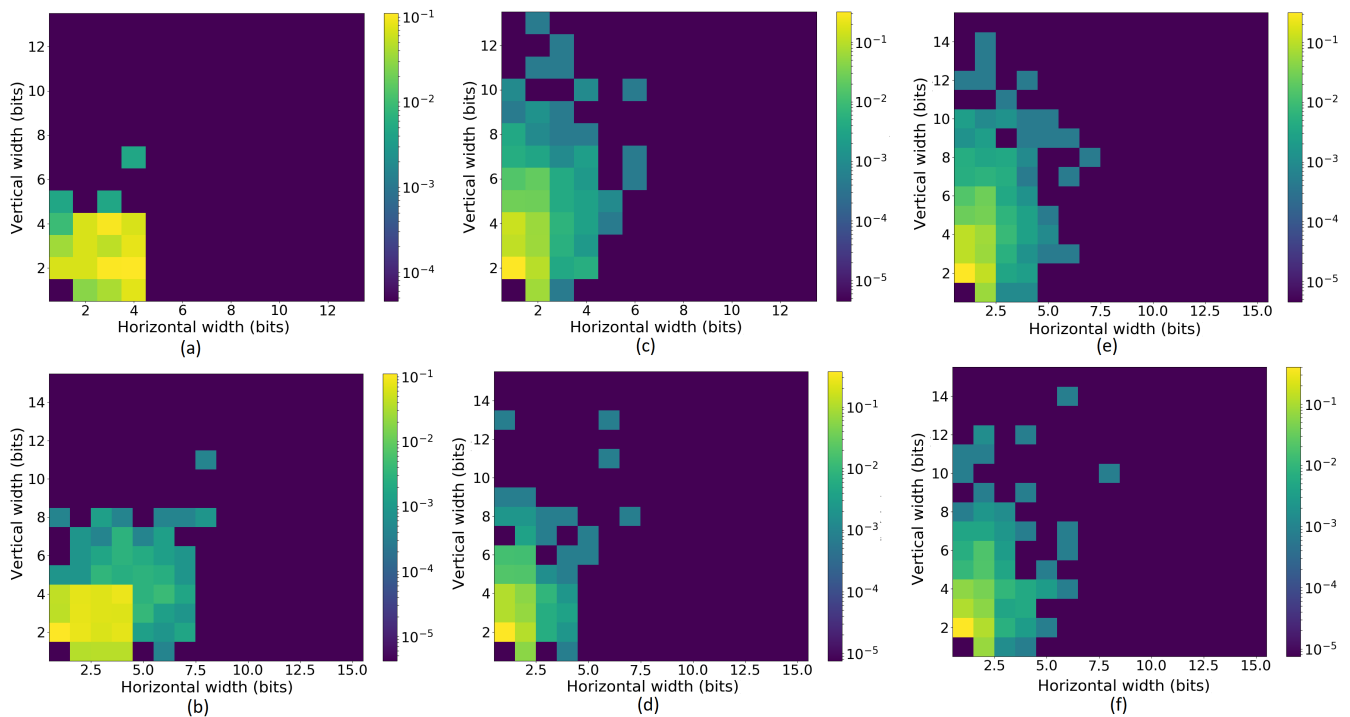


Fig. 14. Heat maps of MCU distributions as a function of their horizontal and vertical extension. Colorscale indicates the normalized counts, i.e., the probability that an MCU would have a certain shape in horizontal and vertical direction. Data collected for the Cypress SRAM for various proton energies at Quirónsalud, bottom plots, and elsewhere, top. In detail: (a) 2.5 MeV protons from CNA, (b) 2.5 MeV protons from Quirónsalud, (c) 124 MeV protons from UMCG, (d) 100 MeV protons from Quirónsalud, (e) 186 MeV protons from UMCG, (f) 226 MeV protons from Quirónsalud.

may be interesting to perform these same measurements in a highly degraded beam from a cyclotron to further enhance this comparison because this degradation technique was previously presented [10] as one that can be very effective at quantifying direct proton ionization phenomena in space when degrading a beam from an initial energy of  $\sim 70$  MeV.

Despite exploiting the physical mapping of the bits in the SRAM, the minimum level of detail that the ESA Monitor provides is down to block of 32 kbits. Therefore, this functionality cannot be used to assess multiple-cell upsets (MCUs). These data are however available for the Cypress SRAM thanks to a collaboration with Laboratoire d'Informatique, de Robotique et de Microélectronique de Montpellier (LIRMM) [25, 26]. Multiple cell-upsets are those that are caused by a single particle strike. They are discriminated based on the physical occurrence of adjacent or quasi-adjacent bits and their simultaneous appearance, which is dictated by the readout frequency.

MCUs are typically classified in terms of multiplicity, i.e., how many bit flips are present in the MCU. However, for high-energy protons, a representation that makes use of other characteristics was found to provide a better description of the types of MCUs that one can get from these particles. This is because the MCUs are here represented with a 2D classification that takes into account the probability of occurrence with respect to the extension of the MCU in the vertical and horizontal directions. The resulting heat maps allow determining the most likely shapes of MCUs in the SRAM under a certain beam.

Fig. 14 depict six of such heat maps. The three on the top were obtained in more standard irradiation facilities in Europe, whereas the three on the bottom were obtained from the data collected at Quirónsalud. Except for case (a) and (b) the energies for the protons at the top and at the bottom are not an exact match, but are assumed to be close enough that no significant variations are expected due to the very low variability of nuclear elastic and inelastic scattering secondary ion compositions among these energies.

Concerning the high energy heat maps, the 100-226 MeV cases portray similar distributions with maximum likelihood for the  $2 \times 1$  MCU and progressively decreasing likelihood as the dimension in x and y increases. There are some small differences in the maximum extension that some very rare events may have, but overall the agreement is very good. This seems to confirm again that no pulsed beam effects were observed.

Concerning the low-energy protons that are collected at 2.5 MeV, note that the proton direct ionization effects seem to be characterized by a square of roughly equal likelihood that extends up to 4 bits in both vertical and horizontal directions. However, for the case in which the 2.5 MeV beam was obtained as mono-energetic, there are basically no outliers outside this square of equal likelihood. On the other hand, for the case in which the 2.5 MeV beam was obtained by degradation from 70 MeV, there is a crown of events of lower likelihood showing that there are MCUs with far larger extensions in both vertical and horizontal directions. This may be an effect of the wider spectrum of protons, but may also



indicate pulsed beam effects from direct proton ionization, which so far were never observed in other facilities. The reason why the second option is considered more likely is because the elastic and inelastic scattering events that are coming from protons of higher energy typically have higher extension in the vertical than the horizontal direction, as also shown in the plots for the high-energy protons. On the other hand, for this run, the symmetry in the distribution among the two directions is maintained, which is something that was not observed before for any other particle type in continuous beams.

To summarize the SEE testing results, the SEU cross sections at high energies were observed to be compatible with those measured elsewhere in cyclotron-based facilities within an error of 33%, that is not due to pulsed beam effects, because it would be expected to result in the opposite effect. The agreement was proven to be good for the standard energy testing range of 20-200 MeV and was also confirmed by verifying the MCU shapes. Concerning the lower energy tests that may be used for direct proton ionization experiments, they cannot be considered fully conclusive. It is clear that having a degraded beam from high-energy provides a different kind of proton spectrum at the DUT than having mono-energetic protons. This may result in measuring lower SEU cross-section. Furthermore, concerning the MCU analysis, some MCU types, that were not observed in previous experiments, may indicate pulsed beam effects.

## V. CONCLUSIONS

High-energy proton beams are in high demand for radiation effect testing, therefore starting to exploit accelerators dedicated to proton therapy for this market may be desirable. The accelerator studied in this paper, at the Quirónsalud proton therapy centre, is based on a synchrocyclotron that posed some unique potential challenges for SEE testing, such as pulsed beam, small spot beam scanning, complex time structure and fixed flux.

Independent measurements performed by CERN to characterize the beam were able to capture the whole time structure of the beam. Despite the beam scanning, the attained beam uniformity was excellent and compliant with needs expressed in standards for electronics testing. SEU cross section characterization measurements on golden chips that were previously characterized in continuous beams also reveal a good agreement when it comes to measuring SEU cross sections at high energies, i.e., 20-200 MeV. No beam pulse effects were observed despite the use of very large instantaneous flux on localized areas of the chips. Underestimations were measured when very low degraded energies are attained, but this is somewhat expected due to the large differences among a monochromatic beam and a wide spectrum beam like that obtained through degradation. These statements are also reinforced by the analysis of MCUs observed in one of the golden chips.

The constraints related to the tuning of the flux may remain a challenge for the testing of some types of devices or some types of complex applications. In spite of this limitation, the facility can be deemed suitable for performing some types of

SEE measurements for qualification purposes for space, accelerator and terrestrial applications. The error rate estimations obtained by measuring SEE cross sections in this facility agree very well with those measured at PSI and UMCG.

## VI. ACKNOWLEDGMENTS

We acknowledge Luigi Dilillo and the LIRMM team at the University of Montpellier, France, for having performed the data analysis required to determine the MCUs from the raw data in our SRAMs. We also acknowledge Helmut Puchner from Infineon, San Jose, CA, USA, for having provided the information required to disable the ECC of the Cypress 65 nm SRAM.

## REFERENCES

- [1] ESCC 25100, "Single event effects test method and guidelines," European Space Components Coordination, ESA, October 2014.
- [2] R. Garcia Alia et al., "Single event effects in high-energy accelerators," *Semicond. Sci. Technol.*, vol. 32, art. no. 034003, Feb. 2017.
- [3] JESD89B International standard, "Measurement and reporting of alpha particle and terrestrial cosmic ray induced soft errors in semiconductor devices," Joint Electron Device Engineering Council (JEDEC), 2021.
- [4] W. Hajdas, F. Burri, C. Eggel, R. Harboe-Sorensen, and R. de Marino, "Radiation effects testing facilities in PSI during implementation of the PROSCAN project," in *IEEE Radiation Effects Data Workshop Rec.*, Phoenix, AZ, USA, July 2002, pp. 160-164.
- [5] E.R. van der Graaf, R.W. Ostendorf, M.J. van Goethem, H.H. Kiewiet, M.A. Hofstee, and S. Brandenburg, "AGORFIRM, the AGOR facility for irradiations of material," in *Proc. 2009 RADECS Conf.*, Bruges, Belgium, Sept. 2009, pp. 451-454.
- [6] M. Rovituso, A. Costantino, T. Borel, W. Van Burik, E. Schenk, and A. Pesce, "The HollandPTC R&D proton beam line for radiation hardness tests in space application," in *Proc. 2022 RADECS Conf.*, Venice, Italy, Oct. 2022.
- [7] K.P. Rodbell, D.F. Heidel, H.H.K. Tang, M.S. Gordon, P. Oldiges, and C.E. Murray, "Low-energy proton-induced single-event-upsets in 65 nm node, silicon-on-insulator, latched and memory cells," *IEEE Trans. Nucl. Sci.*, vol. 54, no. 6, pp. 2474-2479, Dec. 2007.
- [8] D.F. Heidel et al., "Low energy proton single-event-upset test results on 65 nm SOI SRAM," *IEEE Trans. Nucl. Sci.*, vol. 55, no. 6, pp. 3394-3400, Dec. 2008.
- [9] B.D. Sierawski et al., "Impact of low-energy proton induced upsets on test methods and rate predictions," *IEEE Trans. Nucl. Sci.*, vol. 56, no. 6, pp. 3085-3092, Dec. 2009.
- [10] N.A. Dodds et al., "Hardness assurance for proton direct ionization-induced SEEs using a high-energy proton beam," *IEEE Trans. Nucl. Sci.*, vol. 61, no. 6, pp. 2904-2914, Dec. 2014.
- [11] N.A. Dodds et al., "The contribution of low-energy protons to the total on-orbit SEU rate," *IEEE Trans. Nucl. Sci.*, vol. 62, no. 6, pp. 2440-2451, Dec. 2015.
- [12] N.A. Dodds et al., "New insight gained on mechanisms of low-energy proton-induced SEUs by minimizing energy straggle," *IEEE Trans. Nucl. Sci.*, vol. 62, no. 6, pp. 2822-2829, Dec. 2015.
- [13] A. Coronetti et al., "Assessment of proton direct ionization for the radiation hardness assurance of deep sub-micron SRAMs used in space applications," *IEEE Trans. Nucl. Sci.*, vol. 68, no. 5, pp. 937-948, May 2021.
- [14] J.F. Ziegler, and J.P. Biersack, "Stopping and range of ions in matter," <http://www.srim.org>, accessed August 2018.
- [15] C. Cazzaniga et al., "Study of the deposited energy spectra in silicon by high-energy neutron and mixed fields," *IEEE Trans. Nucl. Sci.*, vol. 67, no. 1, pp. 175-180, Jan. 2020.
- [16] C. Cazzaniga et al., "Measurements of ultra-high energy lead ions using silicon and diamond detectors," *Nucl. Instr. Meth. Phys. Res. A*, vol. 985, art. no. 164671, Jan. 2021.
- [17] K. Bilko et al., "Silicon solid-state detectors for monitoring high-energy accelerator mixed field radiation environments," in *Proc. 2021 RADECS Conf.*, Vienna, Austria, Sept. 2021, pp. 179-183.
- [18] C. Cazzaniga et al., "Measurements of low-energy protons using a silicon detector for application to SEE testing," *IEEE Trans. Nucl. Sci.*, vol. 69, no. 3, pp. 485-490, Mar. 2022.

- [19] M. Garcia Diez et al., "Technical note: measurement of the bunch structure of a clinical proton beam using a SiPM coupled to a plastic scintillator with an optical fiber," *Med. Phys.*, vol. 50, no. 5, pp. 3184-3190, Feb. 2023.
- [20] A. Coronetti et al., "SEU characterization of commercial and custom-designed SRAMs based on 90-nm technology and below," in *IEEE Radiation Effects Data Workshop Rec.*, Online conference, Dec. 2020, pp. 56-63.
- [21] A. Coronetti et al., "The pion single-event effect resonance and its impact in an accelerator environment," *IEEE Trans. Nucl. Sci.*, vol. 67, no. 7, pp. 1606-1613, July 2020.
- [22] M.J. Gadlage, A.H. Roach, A.R. Duncan, M.W. Savage, and M.J. Kay, "Electron-induced single-event upsets in 45-nm and 28-nm bulk CMOS SRAM-based FPGAs operating at nominal voltage," *IEEE Trans. Nucl. Sci.*, vol. 62, no. 6, pp. 2717-2724, 2015.
- [23] H. Kettunen et al., "Low energy protons at RADEF - application to advanced eSRAMs," in *IEEE Radiation Effects Data Workshop Rec.*, Paris, France, July 2014, pp. 147-150.
- [24] Y. Morilla et al., "Progress of CNA to become the spanish facility for combined irradiation testing in aerospace," in *Proc. 2018 RADECS Conf.*, Gothenburg, Sweden, Sept. 2018, pp. 250-254.
- [25] G. Tsiligiannis et al., "Multiple cell upset classification in commercial SRAMs," *IEEE Trans. Nucl. Sci.*, vol. 61, no. 4, pp. 1747-1754, Aug. 2014.
- [26] A. Bosser et al., "Investigation on MCU clustering methodologies for cross-section estimation of RAMs," *IEEE Trans. Nucl. Sci.*, vol. 62, no. 6, pp. 2620-2626, Dec. 2015.